The effects of dication symmetry on ionic liquid electrolytes in supercapacitors

2016 J. Phys.: Condens. Matter 28 464005

(http://iopscience.iop.org/0953-8984/28/46/464005)

IOP Publishing Journal of Physics: Condensed Matter
J. Phys.: Condens. Matter **28** (2016) 464005 (9pp) doi:10.1088/0953-8984/28/46/464005

The effects of dication symmetry on ionic liquid electrolytes in supercapacitors

Song Li[1,2], Mengyang Zhu[1,2] and Guang Feng[1,2]

[1] State Key Laboratory of Coal Combustion, School of Energy and Power Engineering, Huazhong University of Science and Technology, Wuhan 430074, People's Republic of China
[2] Nano Interface Center for Energy (NICE), School of Energy and Power Engineering, Huazhong University of Science and Technology, Wuhan 430074, People's Republic of China

E-mail: gfeng@hust.edu.cn

Received 14 January 2016, revised 1 April 2016
Accepted for publication 5 April 2016
Published 14 September 2016

Abstract

The effects of dication symmetry on the structure and capacitance of the electrical double layers (EDLs) of dicationic ionic liquids (DILs) near graphene electrodes were investigated by molecular dynamics (MD) simulation in this work. Symmetrical 1-hexyl-3-dimethylimidazolium di[bis(trifluoromethyl)imide]($[C_6(mim)_2](Tf_2N)_2$) and asymmetrical 1-(1-trimethylammonium-yl-hexyl)-3-methylimidazolium di[bis(trifluoro-methanesulfonyl)-imide] ($[C_6(tma)(mim)](Tf_2N)_2$) were both employed. Radial distribution function (RDF) analysis of the two DILs revealed a shorter distance between the cation–anion pairs in symmetrical $[C_6(mim)_2](Tf_2N)_2$), which was attributed to the closely packed imidazolium ring-anion pairs. In contrast, the trimethylammonium head groups and anions exhibit a relatively longer distance, but a stronger correlation in asymmetrical $[C_6(tma)(mim)](Tf_2N)_2$. In addition, it was illustrated that more symmetrical DIL ions in EDLs are distributed near graphite electrodes and exhibit closer distances to the electrode, which is most probably due to the parallel orientation of imidazolium rings, reducing the distance between the cation and the graphene. In contrast, asymmetrical DILs, with one trimethylammonium head group and one imidazolium ring in the dications, are loosely packed due to their tilting orientation near graphene surfaces. However, the capacitance–potential (C–V) curves of the two DILs are almost the same, regardless of the opposite sign of potential of zero charge (PZC), indicating the insignificant influence of dication symmetry on the capacitance of DIL-based supercapacitors.

Keywords: dicationic ionic liquids, capacitance, electric double layer, supercapacitor

(Some figures may appear in colour only in the online journal)

Introduction

Room temperature ionic liquids (RTILs) are widely used as promising green solvents [1], catalysts [2], lubricants [3], and electrolytes [4] due to their outstanding properties such as low melting point, low volatility, high stability, high miscibility, and wide electrochemical window [5]. In recent years, supercapacitors with RTILs as electrolytes have attracted increasing research interest [6]. One of the research goals is to identify the potential RTIL electrolyte candidates for significantly improving the energy density of supercapacitors. It is known that supercapacitors physically store electric energy in the electric double layer (EDL) formed at charged electrode surfaces. Theoretical studies have reported that the EDL structure in RTIL-based supercapacitors consists of alternative cation and anion layers, and both the ion size/geometry and its charge density may affect EDL formation [7]. Thus, the improved performance of supercapacitors may be achieved by tuning the ion size/geometry or its charge density. In addition, it has been reported that large counter-ions result in lower capacitance [8], which is because larger counter-ions occupying more space decrease the countercharge density in EDLs and thus reduce charge screening efficiency. The relative cation/anion size may also influence the performance of

supercapacitors [9]. When the sizes of cations and anions are approximate, the capacitance–potential (C–V) curve tends to be symmetrical. Otherwise an asymmetrical C–V curve with higher capacitance in either positive or negative potentials can be observed.

Currently, the majority of studies are focused on monocationic ionic liquids (MILs) with the cation carrying one unit charge and associated with one anion. In contrast, dicationic ionic liquids (DILs) are composed of the dication carrying two unit charges and each dication is associated with two anions [10]. Due to their high thermal stability and low volatility, DILs are excellent electrolyte candidates for supercapacitors working at high temperature [11]. Our previous studies by molecular dynamics (MD) simulation have revealed that in comparison with MILs, DILs exhibit less spatial heterogeneity in bulk [12] and a longer life-time of cation–anion pairs [13]. We have also explored the EDLs of DILs in onion-like carbon electrodes. It is demonstrated that the BF_4-containing DIL-based supercapacitor exhibits similar capacitance to the MIL-based one, whereas the Tf_2N-containing DIL-based supercapacitor shows higher capacitance than the MIL-based one, which is consistent with the experimental measurements [14].

All the DILs mentioned above have symmetrical dications, i.e. each dication consists of two identically charged head groups. However, whether the symmetry of the dications will influence the micro-organization of DILs, especially their EDL structure and capacitance, is still unknown. Although there are experimental reports on the physiochemical properties of symmetrical and asymmetrical DILs [15], microscopic investigation into their structural organization and electrochemical performance is still elusive. In this work, MD simulations of the symmetrical (1-hexyl-3-dimethylimidazolium di[bis(trifluoromethyl)imide]) $[C_6(mim)_2](Tf_2N)_2$ and asymmetrical (1-(1-trimethylammonium-yl-hexyl)-3-methylimidazolium di[bis(trifluoromethyl)imide]) $[C_6(tma)(mim)](Tf_2N)_2$ were performed to explore the structural properties of symmetrical and asymmetrical DILs in bulk, and their interfacial behavior in EDLs at graphite electrodes.

Methodology

The force field parameters of symmetrical $[C_6(mim)_2]^{2+}$ and asymmetrical $[C_6(tma)(mim)]^{2+}$ were adapted from the work by Yeganegi [16] and Lopes groups [17], respectively. The force field parameter of the anion $[Tf_2N]^-$ was also obtained from the Lopes group [17]. The force field accuracy was verified by comparing the simulated density of the DILs with experimental data [15]. The van der Waals interaction parameters for carbon in graphite electrodes were taken from Cornell *et al*'s study [18]. All C–H bonds were constrained during the simulation using the LINCS algorithm [19] in order to save CPU time, and a 1.1 nm cutoff was used for the van der Waals interactions. For simulation with electrolyte–electrode systems, long-range electrostatic interactions were treated using the particle mesh Ewald (PME) method [20] with a correction for slab-geometry [21]. The simulation cell is set up as shown in scheme 1. A distance of 7 nm between the positively and negatively charged graphite electrodes was used with a vacuum space of 30 nm (in length) in between. All simulations were performed in a modified version of the MD package Gromacs [22]. A three-layer graphite electrode with a size of 4.18 nm × 4.25 nm was fixed during the simulation. The density of electrolytes in the center of a planar channel cell is tuned to the bulk density. The equilibration was performed in a canonical ensemble at 300 K for 6 ns after annealing from 1000 K to 300 K. All the production runs were then conducted at 300 K. The ensemble temperature was controlled by a Nosé–Hoover thermostat, the most frequently used temperature control scheme in MD simulation. A timestep of 1 fs was applied and the trajectory was saved every 100 fs for computing the number and charge density profiles. A 20 ns production run generated at 300 K was used for further analysis. The averaged number density profiles were calculated along the direction perpendicular to the electrode surface by the binning method.

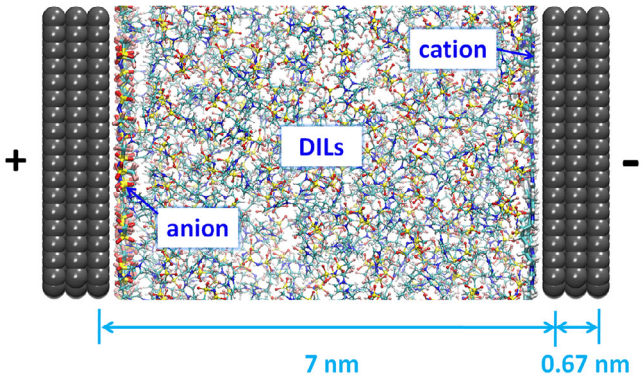

Scheme 1. The schematic representation of a simulation cell for DIL-based supercapacitors in molecular dynamics simulation. The DIL electrolytes were confined by two planar graphene electrodes.

Different electrical potentials were created by uniformly assigning different partial charges to the carbon atoms of the graphene layer in contact with the electrolytes. The potential drop was calculated using the Poisson equation as in a previous study [23]. The differential capacitance–electrical potential (C–V) curve is obtained by fitting the surface charge density versus electric potential using the fifth order polynomials.

Results and discussion

The replacement of one imidazolium (mim) of symmetrical $[C_6(mim)_2](Tf_2N)_2$ with a trimethylammonium (tma) head group may change the structural organization of the DIL. Thus, we first calculated the radial distribution functions (RDFs) of the cation–cation, the cation–anion and the anion–anion pairs of symmetrical $[C_6(mim)_2](Tf_2N)_2$ and asymmetrical $[C_6(tma)(mim)](Tf_2N)_2$ in bulk simulation systems (figure 1). Similar to other RTILs, the cations and anions interact more strongly in comparison to the cation–cation and anion–anion pairs. Although the cation–anion pairs of $[C_6(mim)_2](Tf_2N)_2$ are slightly closer to each other than those of $[C_6(tma)(mim)](Tf_2N)_2$, the peak intensity at approximately 0.5 nm of the cation–anion RDF of $[C_6(mim)_2](Tf_2N)_2$ is lower than that of $[C_6(tma)(mim)](Tf_2N)_2$, suggesting the more condensed

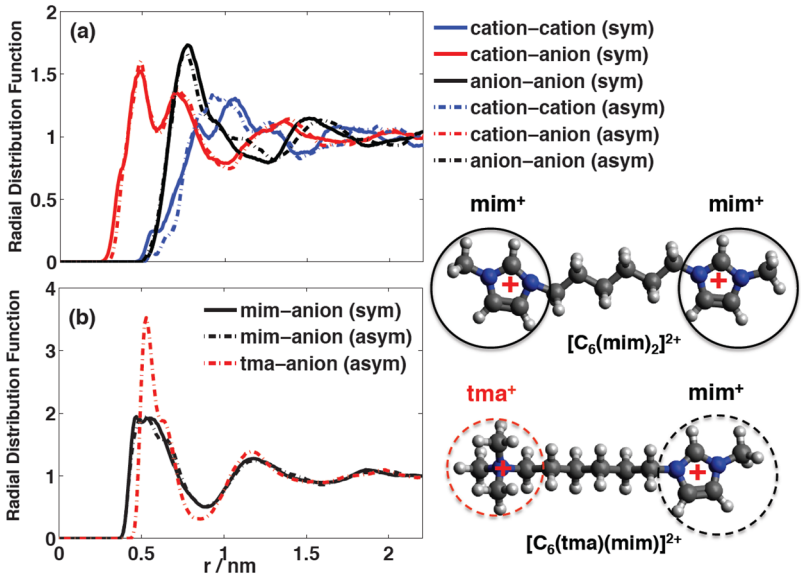

Figure 1. (a) RDFs of cation–cation, cation–anion and anion–anion pairs of symmetrical (sym) $[C_6(mim)_2](Tf_2N)_2$ (in solid line) and asymmetrical (asym) $[C_6(tma)(mim)](Tf_2N)_2$ (in dashed line) at 300 K; (b) RDFs of cation head anion for symmetrical $[C_6(mim)_2](Tf_2N)_2$ (in solid line) and asymmetrical $[C_6(tma)(mim)](Tf_2N)_2$ (in dashed line) at 300 K.

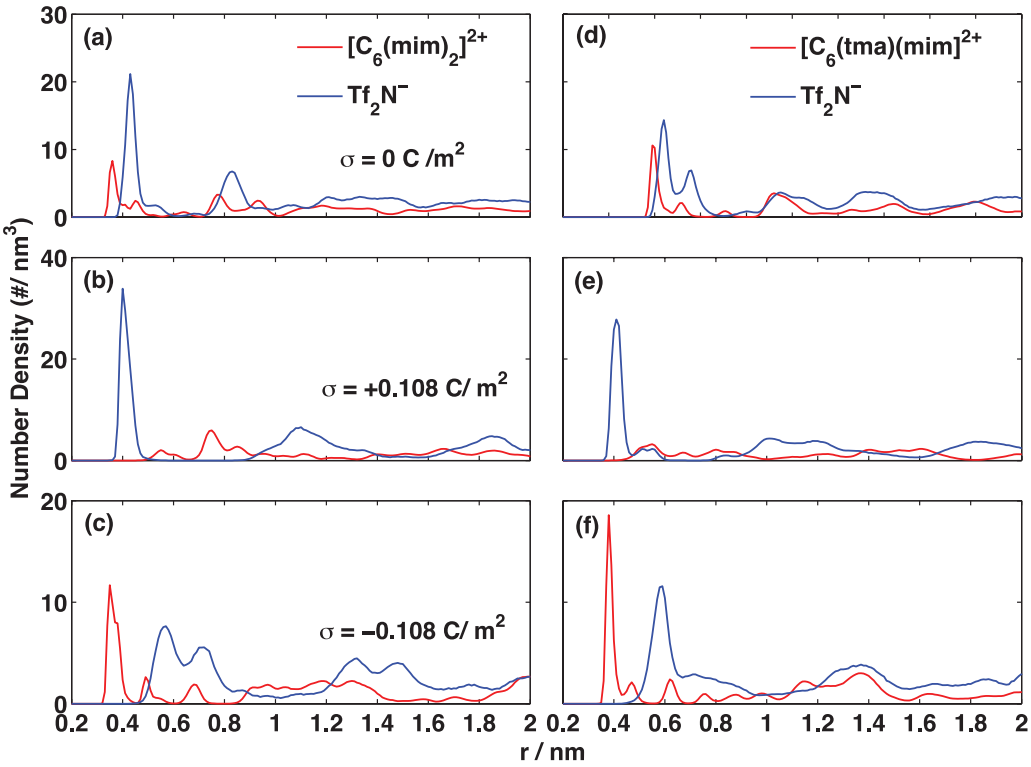

Figure 2. Number density profiles of symmetrical $[C_6(mim)_2](Tf_2N)_2$ ((a)–(c)) and asymmetrical $[C_6(tma)(mim)](Tf_2N)_2$ ((d)–(f)) at the neutral ((a), (d)), positively ((b), (e)) and negatively ((c), (f)) charged graphene electrodes.

packing of cation–anion pairs in asymmetrical $[C_6(tma)(mim)](Tf_2N)_2$ at 0.5 nm. The dissection of cation–anion RDF into imidazolium-anion and tma-anion RDFs shown in figure 1(b) proves that the imidazolium ring-anion distance is shorter than the tma-anion distance, but there is a significantly sharp peak at 0.5 nm in the tma-anion RDF in contrast to the lower peak intensity of the imidazolium-anion RDF, which is consistent with the observation in the cation–anion RDFs of figure 1(a). Similar to cation–anion pairs, the cation–cation pairs of $[C_6(mim)_2](Tf_2N)_2$ are also closer than those of $[C_6(tma)(mim)](Tf_2N)_2$. However, the packing of cation–cation pairs at 0.9 nm is lower. In contrast, the anion–anion interaction of $[C_6(mim)_2](Tf_2N)_2$ is generally comparable with that of $[C_6(tma)(mim)](Tf_2N)_2$, except for a slightly lower peak intensity of $[C_6(tma)(mim)](Tf_2N)_2$ at 0.75 nm. Such observations suggest the more condensed packing of cation–cation and cation–anion pairs as well as the relatively loose packing of anion–anion pairs in the first shell of $[C_6(tma)(mim)](Tf_2N)_2$.

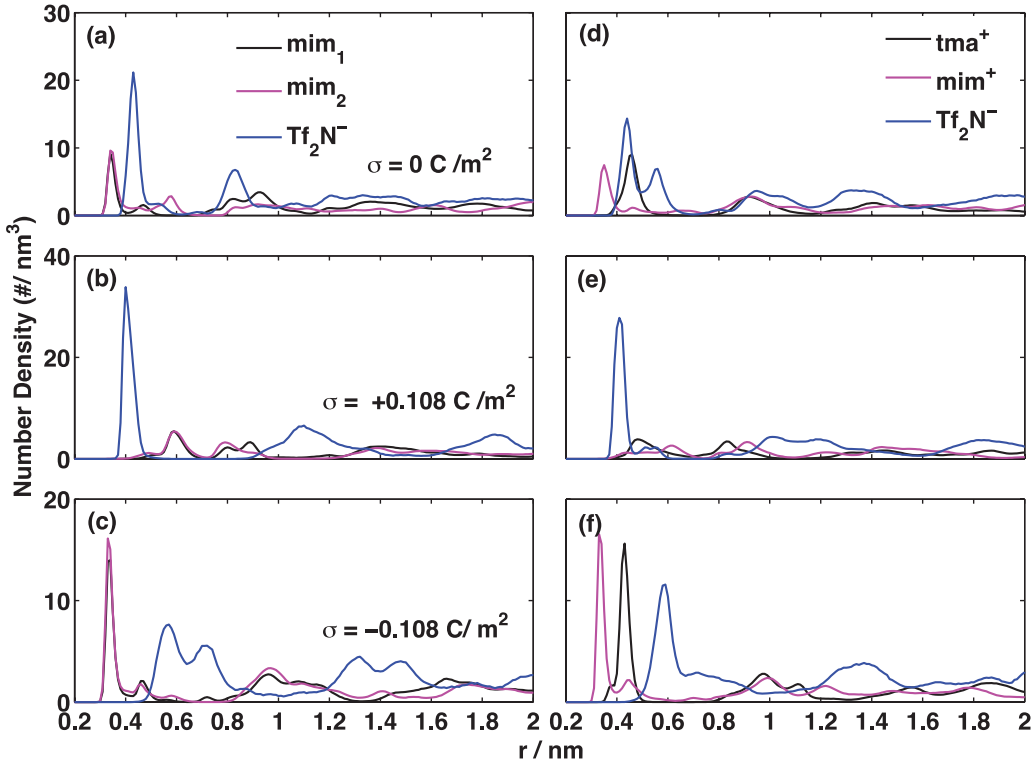

Figure 3. The number density profiles of cation head groups and anions for symmetrical $[C_6(mim)_2](Tf_2N)_2$ ((a)–(c)) and asymmetrical $[C_6(tma)(mim)](Tf_2N)_2$ ((d)–(f)) at neutral ((a), (d)), positively ((b), (e)) and negatively ((c), (f)) charged graphene electrodes at 300 K. In the legend, mim_1 and mim_2 represent the two head rings of the cation $[C_6(mim)_2]^{2+}$.

How can such differences observed in the RDFs of bulk DILs affect their interfacial structure at the graphene electrode? To answer this question, the cation and anion density profiles of $[C_6(mim)_2](Tf_2N)_2$ and $[C_6(tma)(mim)](Tf_2N)_2$ at neutral and charged graphite electrode surfaces have been calculated and shown in figure 2. At the neutral electrode, $[C_6(mim)_2]^{2+}$ (0.38 nm) is slightly closer to the electrode surface than $[C_6(mim)(tma)]^{2+}$ (0.39 nm), which is also true for the anions (0.43 nm versus 0.44 nm). But the number of $[C_6(mim)_2]^{2+}$ (8.2) in the layer ($0 < r \leqslant 0.6$ nm) at the electrode surface is lower than that of $[C_6(mim)(tma)]^{2+}$ (10.1), similar to the anions in the layer of $[C_6(mim)_2](Tf_2N)_2$ (20.2) versus those of $[C_6(tma)(mim)](Tf_2N)_2$ (23.0). At positively charged electrodes (figures 2(b) and (e)), similar amounts of anions of $[C_6(mim)_2](Tf_2N)_2$ (28.3) and those of $[C_6(tma)(mim)](Tf_2N)_2$ (28.6) are packed at the electrode surface with an identical distance to the electrode surface (~0.41 nm). It is also noticed that cations and anions in the EDLs of $[C_6(mim)_2](Tf_2N)_2$ are more efficiently separated than those of $[C_6(tma)(mim)](Tf_2N)_2$, which is probably due to the stronger correlation between the cation–anion pairs of $[C_6(tma)(mim)](Tf_2N)_2$, as observed in the RDFs of figure 1. At the negatively charged electrode (figures 2(c) and (f)), the cations in $[C_6(mim)_2](Tf_2N)_2$ (0.36 nm) are obviously closer to the electrode surface than in $[C_6(tma)(mim)](Tf_2N)_2$ (0.39 nm) and there are more cations of $[C_6(tma)(mim)](Tf_2N)_2$(~13.4) than those of $[C_6(tma)(mim)](Tf_2N)_2$ (~12.4) in the EDL. Considering the number density profile calculated according to the center of mass of dications, the detailed correlation between cations and anions cannot be fully illustrated by figure 2. Thus, the number density based on the center of mass of each cation head group of dications and the anion as a function of the distance from the neutral and charged electrode surface is shown in figure 3.

Comparing symmetrical $[C_6(mim)_2](Tf_2N)_2$ and asymmetrical $[C_6(tma)(mim)](Tf_2N)_2$, the obvious discrepancies are the overlapped density peaks of the two imidazolium heads of $[C_6(mim)_2]^{2+}$ and the separated density peaks of the imidazolium and tma head groups of $[C_6(mim)(tma)]^{2+}$ observed in figure 3. At the neutral electrode, two imidazolium peaks of $[C_6(mim)_2](Tf_2N)_2$ located 0.34 nm from the electrode surface were observed (figure 3(a)). However, for $[C_6(tma)(mim)](Tf_2N)_2$, the imidazolium density peak at 0.35 nm is much closer to the electrode than the tma peak at 0.46 nm in figure 3(d). Such a phenomenon is more significant in the negatively charged electrode due to the strong π–π interaction between imidazolium and graphene [24]. It was also noticed that the intensities of both the imidazolium and tma peaks were enhanced and the location of both peaks toward the negative electrode surface was closer. For $[C_6(mim)_2](Tf_2N)_2$, the imidazolium peaks at 0.33 nm shifted toward the electrode surfaces compared to those at the neutral electrode (figure 3(c)); for $[C_6(tma)(mim)](Tf_2N)_2$, the imidazolium peak at 0.33 nm and the tma peak at 0.38 nm both shifted towards the negatively charged electrode (figure 3(f)).

The 2D ion number density distributions of symmetrical and asymmetrical DILs in the first ion layer (figure 3) were also compared. Different from our previous study on MILs where a highly ordered cation–anion pattern was observed in the first ion layer near the graphene [25], the *XY*-density map

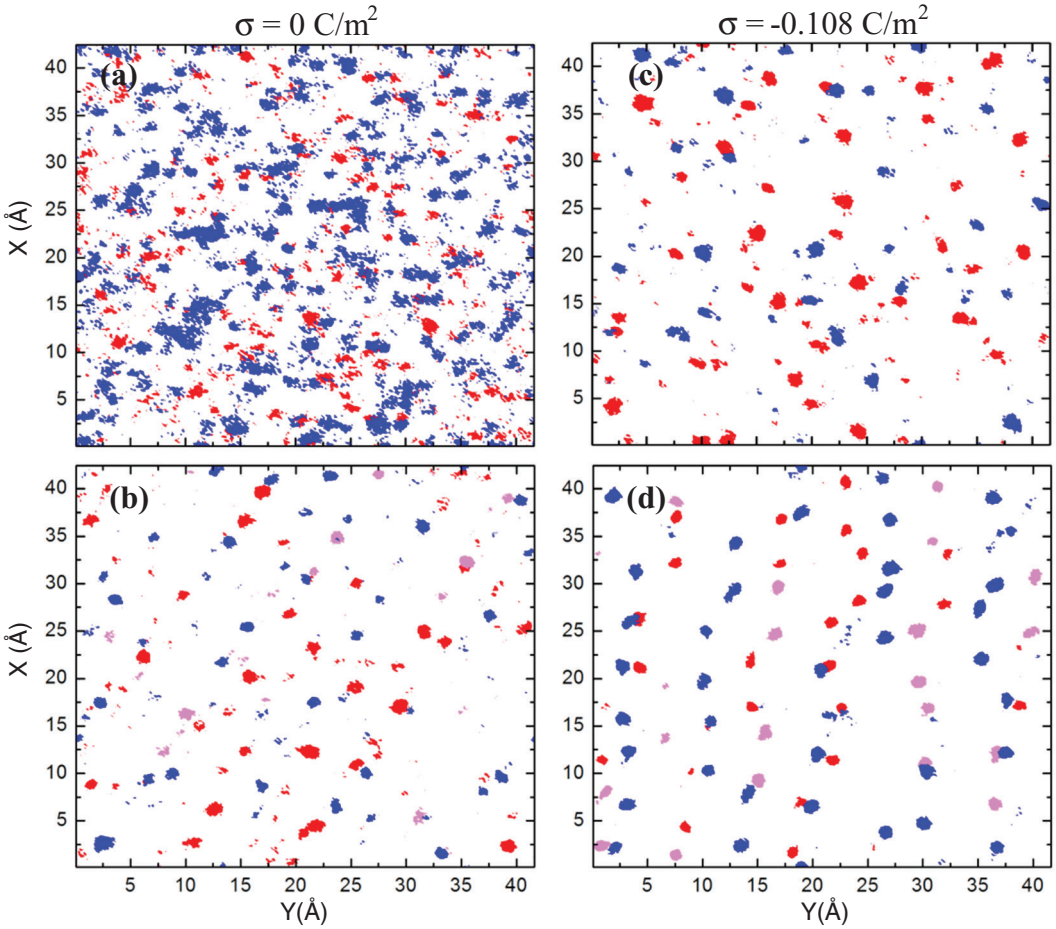

Figure 4. The *XY*-number density map of the cation head (mim^+ in red and tma^+ in magenta) and anion (in blue) in the EDL of $[C_6(mim)_2](Tf_2N)_2$ ((a) and (c)) and $[C_6(tma)(mim)](Tf_2N)_2$ ((b) and (d)) near the neutral and negatively charged graphene electrode. Only the number density of ions above 20% of the maximum density in the map was displayed. The length of *X* and *Y* is in Å.

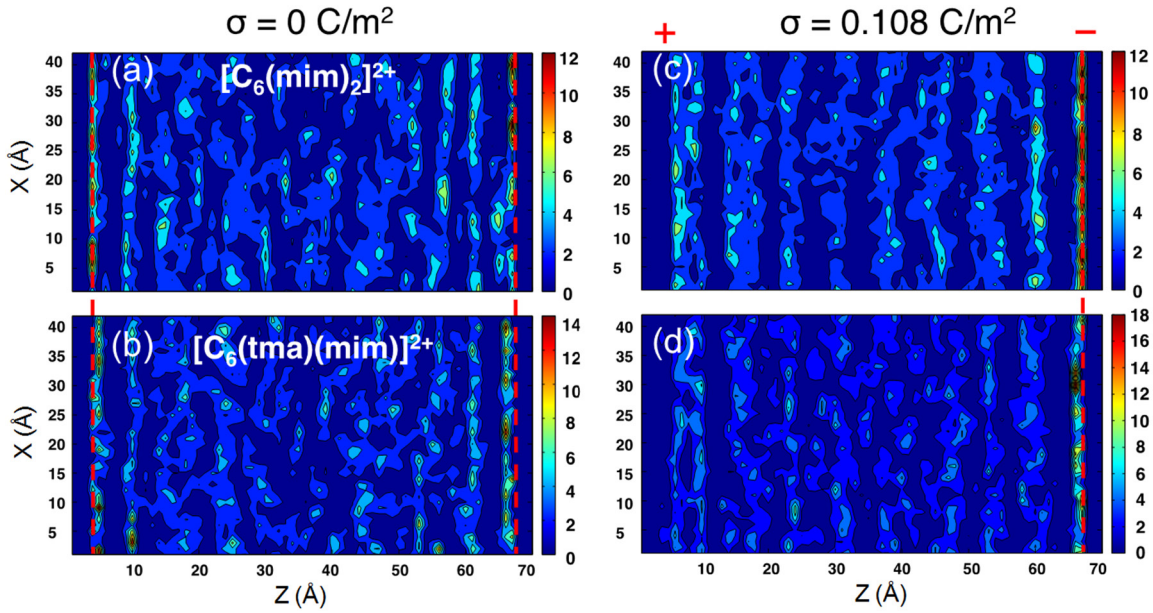

Figure 5. 2D-number density map of the cation head (mim^+ and tma^+ head groups) of $[C_6(mim)_2](Tf_2N)_2$ ((a) and (c)) and $[C_6(tma)(mim)](Tf_2N)_2$ ((b) and (d)) across the neutral and charged graphene-based supercapacitors. The length of *X* and *Z* is in Å.

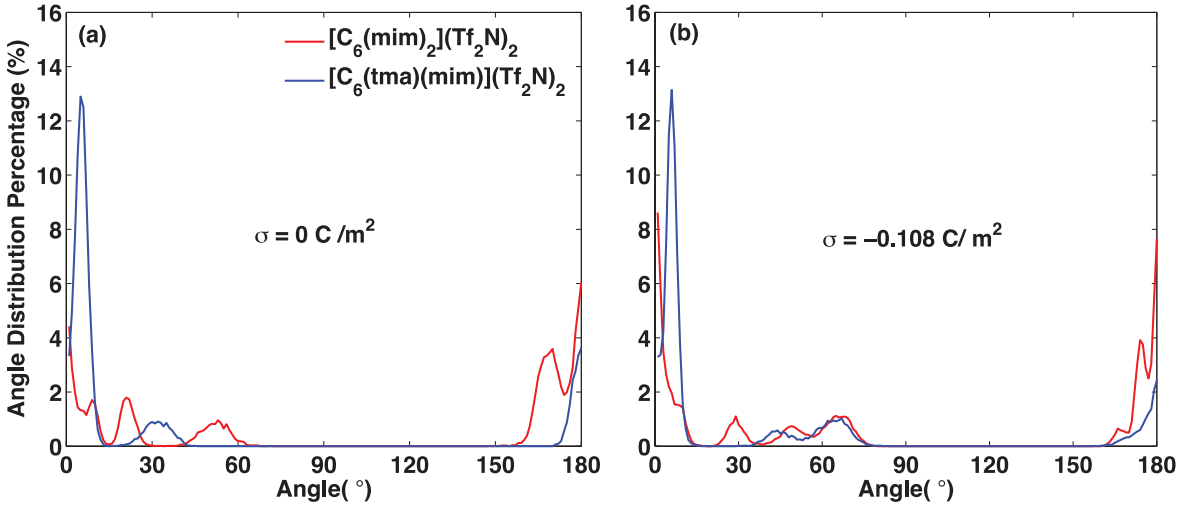

Figure 6. The distribution of the angle formed by the alkyl chain of $[C_6(mim)_2](Tf_2N)_2$ and $[C_6(tma)(mim)](Tf_2N)_2$ of the interfacial layer (0–0.6 nm) with a neutral (a) and a charged graphene surface (b) at 300 K.

of the cation head and anions in the EDLs of the two DILs shown in figure 4 reveals a highly ordered distribution of the cation head and anions of a asymmetrical DIL in contrast to the relatively random distribution of symmetrical $[C_6(mim)_2](Tf_2N)_2$. Once negatively charged, both DILs exhibit enhanced ordering of ion distribution. However, asymmetrical $[C_6(tma)(mim)](Tf_2N)_2$ still presents a highly ordered pattern compared with the symmetrical one. This may be attributed to the more evident correlation between tma^+ and anions, as shown in figures 1(b) and 3(d) and (f), resulting in a well-ordered interfacial microstructure.

The cross-section number density maps based on the cation head groups of two DILs (figure 5) demonstrate the similar interfacial distribution of dications near electrode surfaces, as shown in figure 3. Symmetrical dications $[C_6(mim)_2]^{2+}$ are closer to the electrode than the asymmetrical $[C_6(mim)(tma)]^{2+}$ regardless of the charge status of the electrode surfaces. The overall effect is that symmetrical dication $[C_6(mim)_2]^{2+}$ can be more densely packed onto electrode surfaces in contrast with asymmetrical $[C_6(mim)(tma)]^{2+}$. The above-mentioned observations also suggest that symmetrical $[C_6(mim)_2]^{2+}$ tends to be more parallel to electrode surfaces, while there is a tilting angle between asymmetrical $[C_6(mim)(tma)]^{2+}$ and the electrode surface, as further verified by the angle distribution shown in figure 6.

The angle formed by the alkyl linkage chain of $[C_6(mim)_2](Tf_2N)_2$ and $[C_6(tma)(mim)](Tf_2N)_2$ in the interfacial layer (0–0.6 nm) of dications on the electrode surface proved that the majority of symmetrical $[C_6(mim)_2]^{2+}$ cations (at 0° or 180°) are parallel to the neutral electrode surface (figure 6(a)), similar to the reports on imidazolium-based MILs near carbon [26, 27] or mica surfaces [28]. There is also a considerable fraction of $[C_6(mim)_2]^{2+}$ dications located at 21°, 53° and 170°. However, most of the asymmetrical $[C_6(mim)(tma)]^{2+}$ on the neutral electrode surface exhibits a small angle of approximately 5°, and a small fraction of it is located at 32°. At negatively charged electrodes (figure 6(b)), the fraction of dications located at 0° or 180° in $[C_6(mim)_2]](Tf_2N)_2$ increases from 6% to 9%, indicating that there are more dications parallel to the electrode surface due to the enhanced screening efficiency at negatively charged electrodes. But the peaks originally located at 21° and 53° shifted towards 90°, suggesting an increased tendency of perpendicularity for $[C_6(mim)_2]^{2+}$ at graphene surfaces. Overall, the symmetrical dications, which are parallel or perpendicular to the neutral graphene surface, become more parallel or vertical once the electrode is negatively charged. For $[C_6(mim)(tma)]^{2+}$, the peak at 5° was slightly shifted toward 6°, whereas the peak at 32° at the neutral electrodes becomes a twin peak at 44° and 67° near the negatively charged electrodes, implicating more vertical dications.

Based on the above results, symmetrical $[C_6(mim)_2](Tf_2N)_2$ and asymmetrical $[C_6(tma)(mim)](Tf_2N)_2$ exhibit dissimilar microscopic organization, the interfacial distribution of ions and ion orientation on graphene electrodes. But it is still unknown whether the capacitance of two such DIL-based supercapacitors will be affected by the symmetry of dications. Therefore, the differential capacitance–electrical potential (C–V) curves of symmetrical $[C_6(mim)_2](Tf_2N)_2$ and asymmetrical $[C_6(tma)(mim)](Tf_2N)_2$ electrolyte-based EDLs have been calculated and shown in figure 7(a). Unlike a previous report by Si *et al* stating that MILs with symmetrical and asymmetrical monocations exhibit obviously differently shaped C–V curves [29], the C–V curves of symmetrical dicationic $[C_6(mim)_2](Tf_2N)_2$ and asymmetrical $[C_6(tma)(mim)](Tf_2N)_2$ are similar. At the electrical potential of 0–2 V, the differential capacitance of $[C_6(mim)_2](Tf_2N)_2$ is slightly higher than that of $[C_6(tma)(mim)](Tf_2N)_2$; while beyond 2 V, $[C_6(mim)_2](Tf_2N)_2$ exhibits lower capacitance than $[C_6(tma)(mim)](Tf_2N)_2$. However, $[C_6(tma)(mim)](Tf_2N)_2$ displays higher capacitance than $[C_6(mim)_2](Tf_2N)_2$ throughout the negative potentials. Previous studies [30] have proved that the structure of EDLs is dominated by counterions, i.e. at positively charged electrodes, it is mostly anions that contribute to the EDL structure; at negatively charged electrodes, the EDL is determined by cations. Thus, the numbers of cations and anions of $[C_6(mim)_2](Tf_2N)_2$ and $[C_6(tma)(mim)](Tf_2N)_2$ in EDLs under varying potentials are summarized in

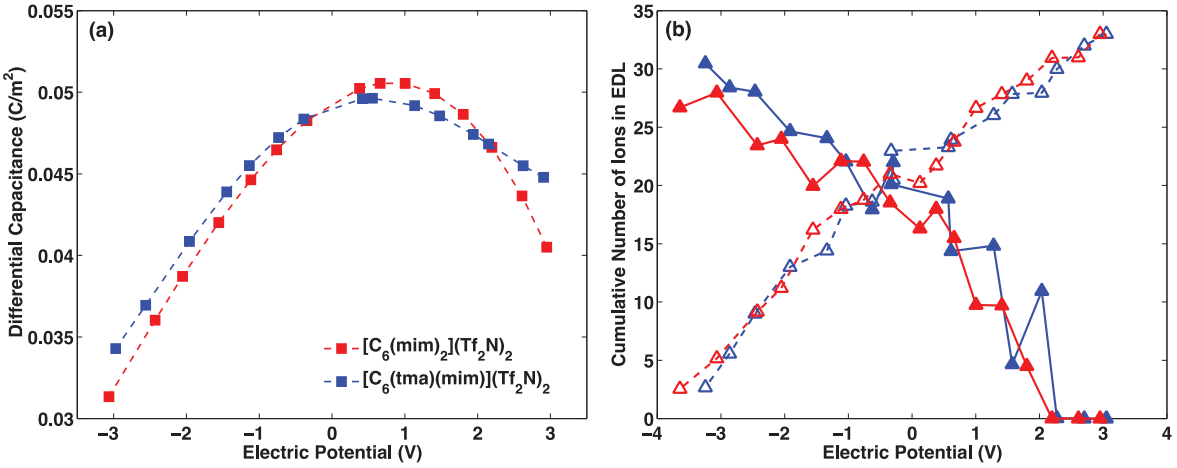

Figure 7. (a) The differential capacitance–electrical potential curves of symmetrical $[C_6(mim)_2](Tf_2N)_2$ and asymmetrical $[C_6(tma)(mim)](Tf_2N)_2$ at 300 K; (b) the cumulative number of cations and anions in the EDLs of $[C_6(mim)_2](Tf_2N)_2$ and $[C_6(tma)(mim)](Tf_2N)_2$ as a function of the electrical potential. Red symbols represent $[C_6(mim)_2](Tf_2N)_2$ and blue symbols represent $[C_6(tma)(mim)](Tf_2N)_2$; the solid lines denote cations and the dashed lines denote anions.

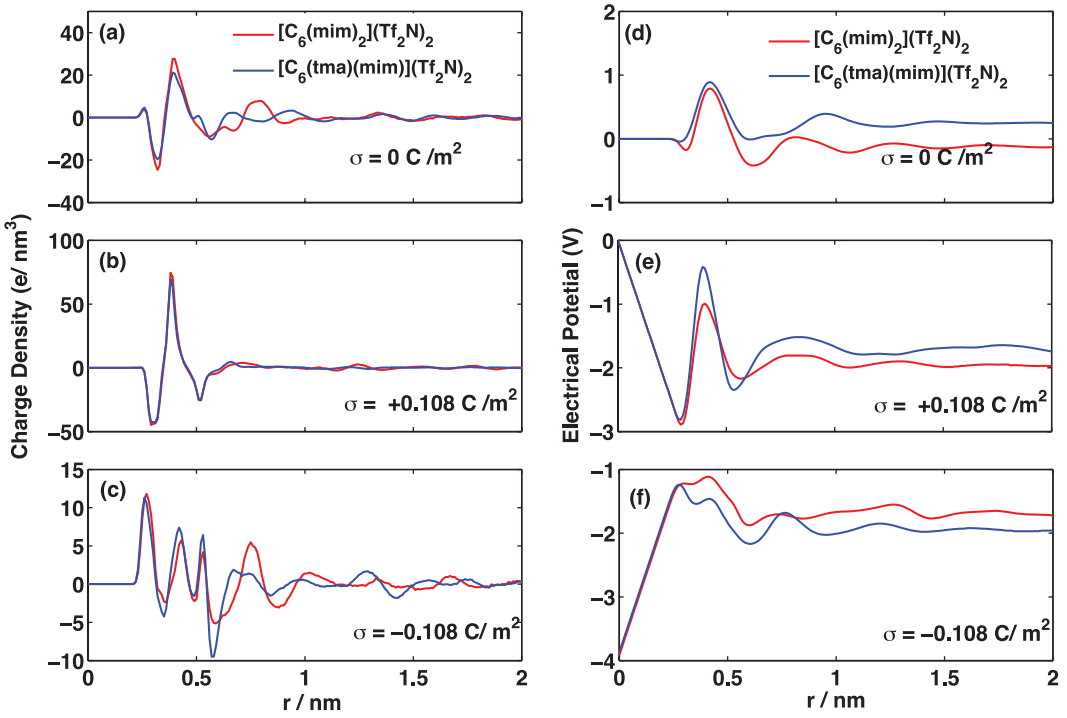

Figure 8. The charge density profiles of the center of mass of $[C_6(mim)_2](Tf_2N)_2$ and $[C_6(tma)(mim)](Tf_2N)_2$ at a neutral (a), positively (b) and negatively (c) charged graphene electrode; the corresponding electrical potential drop of $[C_6(mim)_2](Tf_2N)_2$ and $[C_6(tma)(mim)](Tf_2N)_2$ across the EDL near the neutral (d), positively (e) and negatively (f) charged graphene electrode.

figure 7(b). At positive potentials, the variation in the number of anions from 0 V to 2 V is steeper for $[C_6(mim)_2](Tf_2N)_2$ than for $[C_6(tma)(mim)](Tf_2N)_2$, and beyond 2 V, co-anions are depleted and the number of anions of $[C_6(tma)(mim)](Tf_2N)_2$ rises more sharply than that of $[C_6(mim)_2](Tf_2N)_2$. Such a tendency in the change of cumulative ion number density agrees with the *C–V* curve at positive potentials. At negative potentials, the number of cations in the EDL of $[C_6(tma)(mim)](Tf_2N)_2$ increases more steeply with the electrical potential, leading to a slightly higher capacitance of $[C_6(tma)(mim)](Tf_2N)_2$ at the negative potential than that of $[C_6(mim)_2](Tf_2N)_2$.

Moreover, it is noticed that the potential of zero charge (PZC) of $[C_6(mim)_2](Tf_2N)_2$ is +0.129 V and the PZC of $[C_6(tma)(mim)](Tf_2N)_2$ is −0.329 V. Lauw *et al* reported that a positive PZC suggests the specific adsorption of cations on a neutral electrode surface and a negative PZC implies the specific adsorption of anions [9]. Our result suggests that neutral graphene tends to adsorb $[C_6(mim)_2]^{2+}$ on the surface in the presence of a $[C_6(mim)_2](Tf_2N)_2$ electrolyte [14]. For asymmetrical $[C_6(tma)(mim)](Tf_2N)_2$, the negative PZC indicates the preferential adsorption of the anion $[Tf_2N]^-$ on neutral graphene surfaces. Comparing the charge density profiles of $[C_6(mim)_2](Tf_2N)_2$ and $[C_6(tma)(mim)](Tf_2N)_2$ shown in

figure 8(a), overall, $[C_6(mim)_2](Tf_2N)_2$ was found to exhibit more negative charge density at 0.32 nm within the EDL than $[C_6(tma)(mim)](Tf_2N)_2$, resulting in a positive PZC in contrast to the negative PZC of $[C_6(tma)(mim)](Tf_2N)_2$ (figure 8(d)). Such an observation reveals that the difference in the number of cations and anions compacted into the EDL of $[C_6(mim)_2](Tf_2N)_2$ is more distinct than that of $[C_6(tma)(mim)](Tf_2N)_2$, which is in agreement with the cumulative ion number density in figure 7(b). At the positively charged electrode in figure 8(b), $[C_6(mim)_2](Tf_2N)_2$ exhibits more negative charge density in the first valley of the EDL than $[C_6(tma)(mim)](Tf_2N)_2$, leading to higher electrical potential; at the negatively charged electrode in figure 8(c), $[C_6(mim)_2](Tf_2N)_2$ exhibits more positive charge density than $[C_6(tma)(mim)](Tf_2N)_2$, leading to lower electrical potential and capacitance, consistent with the *C*–*V* curves of figure 7(a).

Conclusion

DILs have been attracting growing research interest due to their outstanding physiochemical properties such as their high stability and an ion density which is more concentrated in the EDLs of supercapacitors than their monocationic counterparts [14]. Previously, the majority of all reported DILs possessed symmetrical dications; in this study, DIL electrolytes with asymmetrical dications were investigated and compared with symmetrical dication-based DILs via MD simulations. The discrepancy in the microstructure organization of symmetrical and asymmetrical DILs is attributed to the different correlations in imidazolium-anions and tma-anions. It was also found that graphene electrodes prefer to adsorb the imidazolium ring in comparison with the tma head, thus symmetrical $[C_6(mim)_2](Tf_2N)_2$ is more densely and closely packed on electrode surfaces than asymmetrical $[C_6(tma)(mim)](Tf_2N)_2$. In addition, the symmetrical $[C_6(mim)_2]^{2+}$ is more parallel to the graphite surface compared with asymmetrical $[C_6(tma)(mim)]^{2+}$. Payal *et al* reported that for alkyl tails with a length shorter than four carbons, the ring plane can either be parallel or perpendicular to the surface. However, for longer tails, the cation ring plane is predominantly parallel to the mica surface [28]. Similarly, the effect of the alkyl chain length on dication orientation is worthy of being investigated in future work. Interestingly, although there are noticeable differences in the microstructural organization and interfacial behavior of symmetrical and asymmetrical DILs, the shapes of the *C*–*V* curves for the two DILs are quite similar, and this can be explained by the cumulative ion number densities in EDLs. However, at present, it is not sensible to conclude that the symmetry of cations exerts negligible effects on the EDL structure, since Si *et al*'s study has revealed the differently shaped *C*–*V* curves in symmetrical and asymmetrical MILs with $[PF_6]^-$ as an anion [29]. Moreover, our conclusion has only been drawn from the two DILs, $[C_6(mim)_2](Tf_2N)_2$ and $[C_6(tma)(mim)](Tf_2N)_2$, and may not hold true for many other types. Either the variations in the alkyl chain length of the dications or the change in the anion type may give rise to different conclusions, requiring further investigation in the follow-up work.

Notes

The authors declare no competing financial interest.

Acknowledgments

We acknowledge funding support from 1. National Natural Science Foundation of China: 51406060; 2. Natural Science Foundation of Hubei Province of China: 2014CFA089; 3. Fundamental Research Funds for the Central Universities: 2015ZZGH008 and 2015TS033. This work was carried out at the National Supercomputer Center in Tianjin, and the calculations were performed on TianHe-1 (A).

References

[1] Earle M J and Seddon K R 2000 Ionic liquids: green solvents for the future *Pure Appl. Chem.* **72** 1391–8
[2] Welton T 2004 Ionic liquids in catalysis *Coord. Chem. Rev.* **248** 2459–77
[3] Zhou F, Liang Y M and Liu W M 2009 Ionic liquid lubricants: designed chemistry for engineering applications *Chem. Soc. Rev.* **38** 2590–9
[4] Lewandowski A, Galinski M and Stepniak I 2006 Ionic liquids as electrolytes *Electrochim. Acta* **51** 5567–80
[5] Taige M and Schubert J S T 2011 Physico-chemical properties of ionic liquids—part I *Ion. Liq. Today* **1–11** 4–10
[6] Brandt A, Pohlmann S, Varzi A, Balducci A and Passerini S 2013 Ionic liquids in supercapacitors *MRS Bull.* **38** 554–9
[7] Fedorov M V and Kornyshev A A 2014 Ionic liquids at electrified interfaces *Chem. Rev.* **114** 2978–3036
[8] Lockett V, Sedev R, Ralston J, Horne M and Rodopoulos T 2008 Differential capacitance of the electrical double layer in imidazolium-based ionic liquids: influence of potential, cation size, and temperature *J. Phys. Chem.* C **112** 7486–95
[9] Lauw Y, Horne M D, Rodopoulos T, Nelson A and Leermakers F A M 2010 Electrical double-layer capacitance in room temperature ionic liquids: ion-size and specific adsorption effects *J. Phys. Chem.* B **114** 11149–54
[10] Anderson J L, Ding R F, Ellern A and Armstrong D W 2005 Structure and properties of high stability geminal dicationic ionic liquids *J. Am. Chem. Soc.* **127** 593–604
[11] Borges R S, Reddy A L M, Rodrigues M-T F, Gullapalli H, Balakrishnan K, Silva G G and Ajayan P M 2013 Supercapacitor operating at 200 degrees Celsius *Sci. Rep.* **3** 2572
[12] Li S, Feng G, Banuelos J L, Rother G, Fulvio P F, Dai S and Cummings P T 2013 Distinctive nanoscale organization of dicationic versus monocationic ionic liquids *J. Phys. Chem.* C **117** 18251–7
[13] Li S, Banuelos J L, Zhang P, Feng G, Dai S, Rother G and Cummings P T 2014 Toward understanding the structural heterogeneity and ion pair stability in dicationic ionic liquids *Soft Matter* **10** 9193–200
[14] Li S, Van Aken K L, McDonough J K, Feng G, Gogotsi Y and Cummings P T 2014 The electrical double layer of dicationic ionic liquids at onion-like carbon surface *J. Phys. Chem.* C **118** 3901–9
[15] Payagala T, Huang J, Breitbach Z S, Sharma P S and Armstrong D W 2007 Unsymmetrical dicationic ionic liquids: manipulation of physicochemical properties using specific structural architectures *Chem. Mater.* **19** 5848–50

[16] Yeganegi S, Soltanabadi A and Farmanzadeh D 2012 Molecular dynamic simulation of dicationic ionic liquids: effects of anions and alkyl chain length on liquid structure and diffusion *J. Phys. Chem.* B **116** 11517–26
[17] Lopes J N C, Deschamps J and Padua A A H 2004 Modeling ionic liquids using a systematic all-atom force field *J. Phys. Chem.* B **108** 2038–47
[18] Cornell W D, Cieplak P, Bayly C I, Gould I R, Merz K M, Ferguson D M, Spellmeyer D C, Fox T, Caldwell J W and Kollman P A A 1995 Second generation force field for the simulation of proteins, nucleic acids, and organic molecules *J. Am. Chem. Soc.* **117** 5179–97
[19] Hess B, Bekker H, Berendsen H J C and Fraaije J G E M 1997 Lincs: a linear constraint solver for molecular simulations *J. Comput. Chem.* **18** 1463–72
[20] Essmann U, Perera L, Berkowitz M L, Darden T, Lee H and Pedersen L G 1995 A smooth particle mesh Ewald method *J. Chem. Phys.* **103** 8577–93
[21] Yeh I C and Berkowitz M L 1999 Ewald summation for systems with slab geometry *J. Chem. Phys.* **111** 3155–62
[22] Berendsen H J C, Vanderspoel D and Vandrunen R 1995 Gromacs—a message-passing parallel molecular-dynamics implementation *Comput. Phys. Commun.* **91** 43–56
[23] Li S, Feng G and Cummings P T 2014 Interfaces of dicationic ionic liquids and graphene: a molecular dynamics simulation study *J. Phys.: Condens. Matter* **26** 284106
[24] Maleki N, Safavi A and Tajabadi F 2006 High-performance carbon composite electrode based on an ionic liquid as a binder *Anal. Chem.* **78** 3820–6
[25] Feng G, Li S, Zhao W and Cummings P T 2015 Microstructure of room temperature ionic liquids at stepped graphite electrodes *AIChE J.* **61** 3022–8
[26] Dou Q, Sha M L, Fu H Y and Wu G Z 2011 Molecular dynamics simulation of the interfacial structure of $[C_{(N)}Mim][PF_6]$ adsorbed on a graphite surface: effects of temperature and alkyl chain length *J. Phys.: Condens. Matter* **23** 175001
[27] Romero C, Moore H J, Lee T R and Baldelli S 2007 Orientation of 1-butyl-3-methylimidazolium based ionic liquids at a hydrophobic quartz interface using sum frequency generation spectroscopy *J. Phys. Chem.* C **111** 240–7
[28] Payal R S and Balasubramanian S 2014 Effect of cation symmetry on the organization of ionic liquids near a charged mica surface *J. Phys.: Condens. Matter* **26** 284101
[29] Si X J, Li S, Wang Y L, Ye S H and Yan T Y 2012 Effects of specific adsorption on the differential capacitance of imidazolium-based ionic liquid electrolytes *ChemPhysChem* **13** 1671–6
[30] Feng G, Zhang J S and Qiao R 2009 Microstructure and capacitance of the electrical double layers at the interface of ionic liquids and planar electrodes *J. Phys. Chem.* C **113** 4549–59